

12 The Numerical Renormalization Group

Ralf Bulla

Institut für Theoretische Physik

Universität zu Köln

Contents

| | | |
|----------|--------------------------------------------|-----------|
| 1 | Introduction | 2 |
| 2 | The single-impurity Anderson model | 3 |
| 3 | The numerical renormalization group | 8 |
| 3.1 | Logarithmic discretization | 8 |
| 3.2 | Mapping on a semi-infinite chain | 11 |
| 3.3 | Iterative diagonalization | 13 |
| 3.4 | Renormalization group flow | 18 |
| 4 | Final remarks | 20 |

1 Introduction

In the preceding lecture notes by F. Anders you find an introduction to the Kondo effect and quantum impurity systems in general, along with the quantum mechanical models which are supposed to explain the phenomena observed in these systems. Some intuition is required to formulate these models, but the phenomena cannot be read off by just looking at the model Hamiltonian. To actually see the screening of the impurity magnetic moment below the Kondo temperature T_K we need (more or less) sophisticated techniques, and in the context of quantum impurity systems it is the Numerical Renormalization Group method (NRG, developed by K.G. Wilson in the early 1970's [1]) which helped a lot in understanding the Kondo and related effects.¹

The NRG method is special compared to other methods (such as Quantum Monte Carlo) as it is designed exclusively for quantum impurity systems, with a small impurity – an object with a small number of degrees of freedom with arbitrary interactions – coupled to a non-interacting bath – usually a free conduction band, that is non-interacting fermions. Nevertheless, there is an enormous range of physical phenomena which can be realized in such systems, and to which the NRG has been applied. For an overview, see the review Ref. [4] and the hints for further reading in the final section.

In these lecture notes, we will purely focus on the single-impurity Anderson model, to be introduced in Sec. 2, for which all the technicalities of the NRG can be explained without the complications of multi-impurity or multi-channel systems. The single-impurity Anderson model has also been used as a prototype model in Sec. II of the NRG-review [4], and I will use basically the same notation here in the lecture notes.

Any introduction to the NRG method will go through the basic steps of logarithmic discretization, mapping onto a semi-infinite chain, iterative diagonalization and so on, and, of course, you will find precisely this structure in Sec. 2 (Figure 1 illustrates the initial steps of the NRG procedure). These technical steps can be understood with a background in quantum mechanics, in particular some experience in working with creation and annihilation operators for fermions ($c_{i\sigma}^\dagger/c_{i\sigma}$, see below), but even if each single step is clear, beginners in the field very often find it difficult to see the overall picture. I will try to convince the reader that there is indeed a general strategy behind the NRG approach, and that each individual step has its purpose.

There is one issue which very often leads to confusion: that is the role of geometry and the dimension of the bath in which the impurity is embedded. One frequently encounters correlated electron systems in which the dimension is crucial for the physical properties, but for quantum impurity systems you can find remarks in the literature saying that the impurity couples to a single channel only, so it is effectively a one-dimensional problem, possibly like the semi-infinite chain as depicted in Fig. 1c. So if the dimension does not play a role at all, you might want to define the model directly on a semi-infinite chain – I hope these lecture notes will help to clarify this issue.

¹Of course, the NRG is not the only method which can be successfully applied to quantum impurity systems; for an overview see the lecture notes from last year's autumn school [2] and A.C. Hewson's book [3]

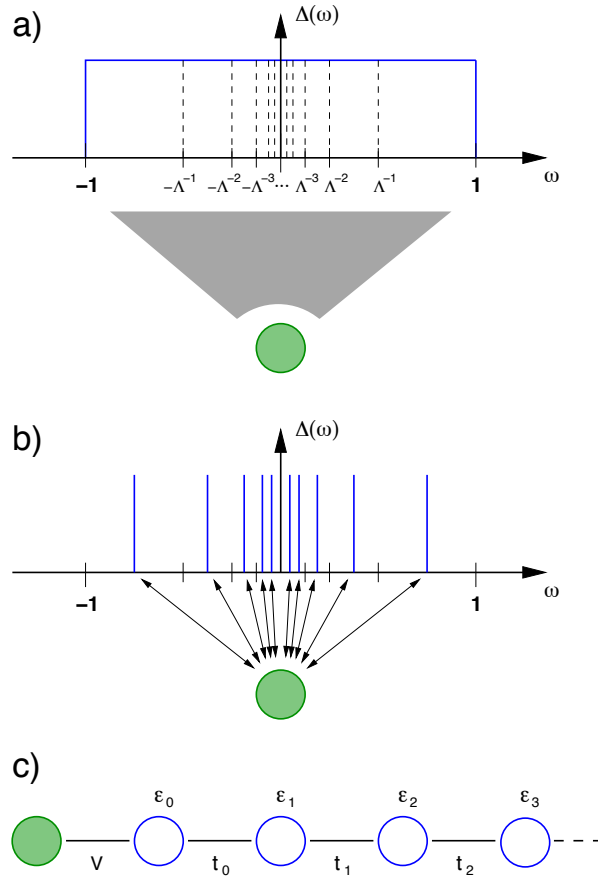


Fig. 1: Initial steps of the NRG illustrated for the single-impurity Anderson model in which an impurity (filled circle) couples to a continuous conduction band via the hybridization function $\Delta(\omega)$; a) a logarithmic set of intervals is introduced through the NRG discretization parameter Λ ; b) the continuous spectrum within each of these intervals is approximated by a single state; c) the resulting discretized model is mapped onto a semi-infinite chain where the impurity couples to the first conduction electron site via the hybridization V ; the parameters of the tight-binding model (see Eq. (38)) are ε_n and t_n . Figure taken from Ref. [4].

2 The single-impurity Anderson model

The Hamiltonian of a general quantum impurity model consists of three parts, the impurity H_{imp} , the bath H_{bath} , and the coupling between impurity and bath, $H_{\text{imp-bath}}$:

$$H = H_{\text{imp}} + H_{\text{bath}} + H_{\text{imp-bath}}. \quad (1)$$

In the single-impurity Anderson model (siAm, Ref. [5]), the impurity consists of a single level with energy ε_f . The Coulomb repulsion between two electrons occupying this level (which then must have opposite spin, $\sigma = \uparrow$ and $\sigma = \downarrow$) is given by U . All the Hamiltonians appearing in these lecture notes are most conveniently written in second quantization, so we have

$$H_{\text{imp}} = \sum_{\sigma} \varepsilon_f f_{\sigma}^{\dagger} f_{\sigma} + U f_{\uparrow}^{\dagger} f_{\uparrow} f_{\downarrow}^{\dagger} f_{\downarrow}, \quad (2)$$

with $f_{\sigma}^{(\dagger)}$ annihilation (creation) operators for a fermion with spin σ on the impurity level.

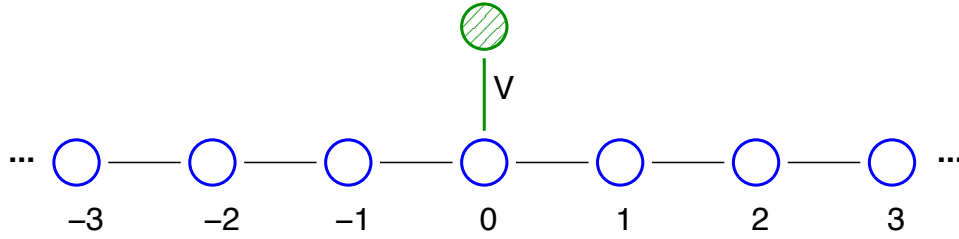


Fig. 2: One possible realization of the single-impurity Anderson model in which the impurity couples to one site (site ‘0’) of a one-dimensional tight-binding chain.

Let us start with a specific geometry of the bath, that is a one-dimensional chain as shown in Fig. 2, with hopping between nearest neighbours (matrix element t_l) and on-site energies ε_l , so we have

$$H_{\text{bath}} = \sum_{\sigma} \sum_{l=-\infty}^{\infty} \varepsilon_l c_{l\sigma}^{\dagger} c_{l\sigma} + \sum_{\sigma} \sum_{l=-\infty}^{\infty} t_l \left(c_{l\sigma}^{\dagger} c_{l+1\sigma} + c_{l+1\sigma}^{\dagger} c_{l\sigma} \right). \quad (3)$$

The operators for the states at site l of the chain are denoted as $c_{l\sigma}^{(\dagger)}$. Note that there is no interaction term between the band states, which is first of all an assumption, but is actually necessary to perform the transformations to be described below.

As indicated in Fig. 2, the impurity only couples to the bath state at site $l = 0$, and in the siAm the form of this coupling is given by

$$H_{\text{imp-bath}} = V \sum_{\sigma} \left(f_{\sigma}^{\dagger} c_{0\sigma} + c_{0\sigma}^{\dagger} f_{\sigma} \right), \quad (4)$$

corresponding to a hybridization of the respective states, with V the hybridization strength.

One might want to set the parameters ε_l and t_l in Eq. (3) to a constant value, which simplifies the calculation, but in general, ε_l and t_l can be site-dependent and, for example, describe a one-dimensional disordered system.

Let us now generalize the model to an arbitrary non-interacting bath. The operators H_{imp} and $H_{\text{imp-bath}}$ are still given by eqs. (2) and (4), respectively, and H_{bath} now has the form

$$H_{\text{bath}} = \sum_{\sigma} \sum_l \varepsilon_l c_{l\sigma}^{\dagger} c_{l\sigma} + \sum_{\sigma} \sum_{ij} t_{ij} \left(c_{i\sigma}^{\dagger} c_{j\sigma} + c_{j\sigma}^{\dagger} c_{i\sigma} \right). \quad (5)$$

For later use we write H_{bath} in the form

$$H_{\text{bath}} = \sum_{\sigma} \vec{c}_{\sigma}^{\dagger} T \vec{c}_{\sigma}, \quad (6)$$

with

$$\vec{c}_{\sigma}^{\dagger} = \left(\dots, c_{-1\sigma}^{\dagger}, c_{0\sigma}^{\dagger}, c_{1\sigma}^{\dagger}, \dots \right), \quad (7)$$

and the matrix elements of T built up by the ε_l and t_{ij} in Eq. (5).

The site index of the operators $c_{l\sigma}^{(\dagger)}$ now runs over all sites of an arbitrary geometry, for example, the two-dimensional lattice as shown in Fig. 3, and t_{ij} is the hopping between any pair (i, j) of

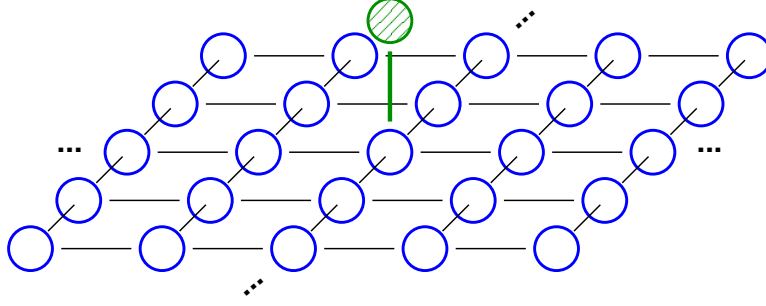


Fig. 3: In this geometry, the impurity couples to one site of a two-dimensional lattice of conduction electrons.

the bath states. The bath might have a complicated structure, but as it is non-interacting, it can always be written in a diagonal form:

$$H_{\text{bath}} = \sum_{\sigma k} \varepsilon_k b_{k\sigma}^\dagger b_{k\sigma}, \quad (8)$$

with the operators $c_{i\sigma}^{(\dagger)}$ and $b_{k\sigma}^{(\dagger)}$ related via a unitary transformation

$$c_{i\sigma} = \sum_k a_{ik} b_{k\sigma}, \quad c_{i\sigma}^\dagger = \sum_k a_{ik}^* b_{k\sigma}^\dagger. \quad (9)$$

The a_{ik} are the matrix elements of the unitary matrix A which diagonalizes the matrix T as defined above

$$(A^t T A)_{kq} = \varepsilon_k \delta_{kq}. \quad (10)$$

The actual diagonalization of the matrix T is, of course, limited by the size of the matrices which can be handled by the computer, but for now it is sufficient to assume that the diagonalization can be done in principle.

Inserting Eq. (9) for $i = 0$ into $H_{\text{imp-bath}}$ from Eq. (4) gives the following form for the hybridization term

$$H_{\text{imp-bath}} = \sum_{k\sigma} V_k \left(f_\sigma^\dagger b_{k\sigma} + b_{k\sigma}^\dagger f_\sigma \right), \quad (11)$$

with $V_k = V a_{0k}$. Let us denote the Hamiltonian written with the operators $b_{k\sigma}^{(\dagger)}$, that is H_{imp} together with H_{bath} Eq. (8) and $H_{\text{imp-bath}}$ Eq. (11), as the k -representation of the siAm, in contrast to the site-representation, eqs. (4,5).

We can now easily calculate the form of the hybridization function using equations of motion. This is described in detail in Ref. [6] and shall not be repeated here. The essential point is that the one-particle Green function $G_\sigma(z) = \langle\langle f_\sigma, f_\sigma^\dagger \rangle\rangle_z$ can be written in the form

$$G_\sigma(z) = \frac{1}{z - \varepsilon_f - \bar{\Delta}(z) - \Sigma^U(z)}, \quad (z = \omega + i\delta), \quad (12)$$

with $\Sigma^U(z)$ the correlation part of the one-particle self energy and the hybridization function

$$\bar{\Delta}(z) = \sum_k V_k^2 \frac{1}{z - \varepsilon_k}. \quad (13)$$

Usually it is the imaginary part of this quantity which is referred to as the hybridization function:

$$\Delta(\omega) = -\lim_{\delta \rightarrow 0} \text{Im} [\bar{\Delta}(z = \omega + i\delta)] = \pi \sum_k V_k^2 \delta(\omega - \varepsilon_k), \quad (14)$$

with the second equality following from Eq. (13). In any case, it is this single frequency dependent quantity in which all the details of the bath are encoded, or, in other words, all that the impurity sees from the bath is the hybridization function $\Delta(\omega)$. This can also be shown more formally by starting from the functional integral for the k -representation of the siAm, and by integrating out the conduction electron degrees of freedom (this can be done analytically, since the conduction electrons are non-interacting). The effective action for the impurity degree of freedom then contains the $\Delta(\omega)$ as the only remnant of the bath.

We are now able – at least in principle – to calculate the hybridization function for any given geometry, but can this be reversed? Is it possible to deduce the precise form of the siAm in the site representation, that is all the ε_l and t_{ij} in Eq. (5) purely from the form of $\Delta(\omega)$? This is, in fact, not the case, and to see this let us have a look at the siAm defined for a semi-infinite chain as shown in Fig. 4, with

$$H_{\text{bath}} = \sum_{\sigma} \sum_{l=0}^{\infty} \varepsilon_l c_{l\sigma}^{\dagger} c_{l\sigma} + \sum_{\sigma} \sum_{l=0}^{\infty} t_l \left(c_{l\sigma}^{\dagger} c_{l+1\sigma} + c_{l+1\sigma}^{\dagger} c_{l\sigma} \right), \quad (15)$$

and $H_{\text{imp-bath}}$ given by Eq. (4).

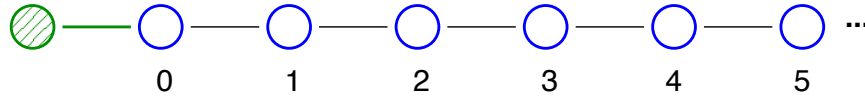


Fig. 4: In this geometry, the impurity couples to the first site of a semi-infinite chain of conduction electrons.

There is a straightforward procedure (‘continued fraction expansion’) to calculate, for a given $\Delta(\omega)$, the set of parameters $\{\varepsilon_l\}$ and $\{t_l\}$ of this semi-infinite chain. This means that we can start, for example, with a two-dimensional model as in Fig. 3, calculate the $\Delta(\omega)$ for this geometry, and then calculate the $\{\varepsilon_l\}$ and $\{t_l\}$ for the semi-infinite chain via a continued fraction expansion. The resulting model looks different, apparently, but for the impurity all that counts is the hybridization function and this is the same for both models. In this sense the siAm is said to be effectively a one-dimensional problem and we can view the chain in Fig. 4 as the single channel the impurity is coupling to.

A side remark: the calculation of $\Delta(\omega)$ for the siAm given in the form of a semi-infinite chain is rather simple, as it can be cast in the form of a continued fraction

$$\Delta(z) = \frac{V^2}{z - \varepsilon_0 - \frac{t_0^2}{z - \varepsilon_1 - \frac{t_1^2}{z - \varepsilon_2 - \frac{t_2^2}{z - \varepsilon_3 - \dots}}}}. \quad (16)$$

In the site representation, we have so far considered a coupling of the impurity to a single site, as in Figs. 2 and 3. Let us now generalize this to

$$H_{\text{imp-bath}} = \sum_{\sigma m} V_m (f_{\sigma}^{\dagger} c_{m\sigma} + c_{m\sigma}^{\dagger} f_{\sigma}) , \quad (17)$$

that is a coupling to the sites m with hybridization strength V_m . Figure 5 shows a possible realization.

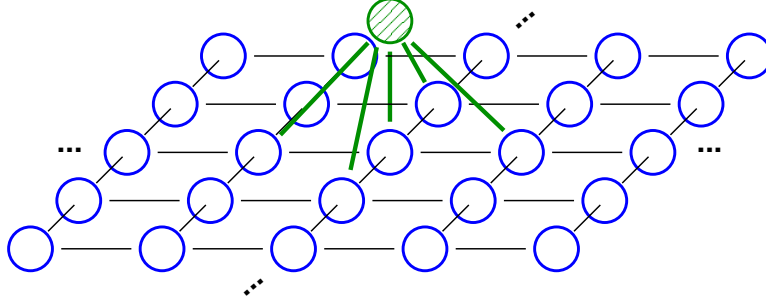


Fig. 5: In this geometry, the impurity couples to one site plus the four nearest neighbours of this site of a two-dimensional lattice of conduction electrons.

We can now insert Eq. (9) for $i = m$ into this expression and arrive at the same form of $H_{\text{imp-bath}}$ Eq. (11) as above, with $V_k = \sum_m V_m a_{mk}$. The structure of the Hamiltonian in the k -representation is thus exactly the same as before.

Before we continue, let us summarize what we have learned so far. Whatever the geometry of the siAm, one can always write the model in the k -representation eqs. (8,11) (from which the form of $\Delta(\omega)$ follows directly) or as a semi-infinite chain. The actual calculation of $\Delta(\omega)$ can be done in various ways – in the simplest case H_{bath} is translationally invariant and the diagonalization of H_{bath} can be done via Fourier transformation, but in the general case one cannot avoid diagonalizing large matrices. Leaving aside these technical issues, we have obtained a quantity which completely characterizes the impurity-bath coupling, so the next question is, what $\Delta(\omega)$ can tell us about Kondo physics. The important feature here is the behaviour of $\Delta(\omega)$ for $\omega \rightarrow 0$. Standard Kondo physics requires $\Delta(\omega \rightarrow 0) \neq 0$, whereas the situation is more complex if $\Delta(\omega) \propto |\omega|^r$ for $\omega \rightarrow 0$, with an exponent $r > -1$ (see the discussion in Sec. IV.C.2 of Ref. [4]).

We have now seen various ways to write the siAm, but the actual starting point for the NRG procedure has not been introduced yet. This is the Hamiltonian in the ‘integral representation’

$$\begin{aligned} H_{\text{bath}} &= \sum_{\sigma} \int_{-1}^1 d\varepsilon g(\varepsilon) a_{\varepsilon\sigma}^{\dagger} a_{\varepsilon\sigma} , \\ H_{\text{imp-bath}} &= \sum_{\sigma} \int_{-1}^1 d\varepsilon h(\varepsilon) \left(f_{\sigma}^{\dagger} a_{\varepsilon\sigma} + a_{\varepsilon\sigma}^{\dagger} f_{\sigma} \right). \end{aligned} \quad (18)$$

The conduction band is now assumed to be continuous, with the band operators satisfying the standard fermionic commutation relations: $[a_{\varepsilon\sigma}^{\dagger}, a_{\varepsilon'\sigma'}]_{+} = \delta(\varepsilon - \vare')\delta_{\sigma\sigma'}$. The dispersion of the

band is given by $g(\varepsilon)$, with the band cutoffs set to -1 and 1 (for simplicity). The hybridization between the impurity and the band states is given by $h(\varepsilon)$.

The calculation of the hybridization function for the model in this form works in the same way as for the k -representation, Eq. (14). The result is

$$\Delta(\omega) = \pi \int_{-1}^1 d\varepsilon h(\varepsilon)^2 \delta(\omega - g(\varepsilon)) = \pi h(g^{-1}(\omega))^2 \frac{d}{d\omega} g^{-1}(\omega) , \quad (19)$$

with $g^{-1}(\omega)$ the inverse function of $g(\varepsilon)$, that is $g^{-1}(g(\varepsilon)) = \varepsilon$. Now remember that the relevant quantity is the hybridization function $\Delta(\omega)$, given by the specific geometries as discussed above. For a given $\Delta(\omega)$, there are obviously many ways to divide the ω -dependence between $g^{-1}(\omega)$ and $h(g^{-1}(\omega))$, corresponding to different ways of dividing the ε -dependence between $g(\varepsilon)$ and $h(\varepsilon)$. This feature will be useful later.

With the siAm in the integral representation eqs. (18) we can now turn to the NRG treatment of the model.

3 The numerical renormalization group

3.1 Logarithmic discretization

The Hamiltonian in the integral representation Eq. (18) is a convenient starting point for the logarithmic discretization of the conduction band. As shown in Fig. 1a, the parameter $\Lambda > 1$ defines a set of intervals with discretization points

$$x_n = \pm \Lambda^{-n} , \quad n = 0, 1, 2, \dots . \quad (20)$$

The width of the intervals is given by

$$d_n = \Lambda^{-n} (1 - \Lambda^{-1}) . \quad (21)$$

Within each interval we introduce a complete set of orthonormal functions

$$\psi_{np}^{\pm}(\varepsilon) = \begin{cases} \frac{1}{\sqrt{d_n}} e^{\pm i\omega_n p \varepsilon} & \text{for } x_{n+1} < \pm \varepsilon < x_n \\ 0 & \text{outside this interval .} \end{cases} \quad (22)$$

The index p takes all integer values between $-\infty$ and $+\infty$, and the fundamental frequencies for each interval are given by $\omega_n = 2\pi/d_n$. The next step is to expand the conduction electron operators $a_{\varepsilon\sigma}$ in this basis, i.e.

$$a_{\varepsilon\sigma} = \sum_{np} \left[a_{np\sigma} \psi_{np}^+(\varepsilon) + b_{np\sigma} \psi_{np}^-(\varepsilon) \right] , \quad (23)$$

which corresponds to a Fourier expansion in each of the intervals. The inverse transformation reads

$$\begin{aligned} a_{np\sigma} &= \int_{-1}^1 d\varepsilon [\psi_{np}^+(\varepsilon)]^* a_{\varepsilon\sigma} , \\ b_{np\sigma} &= \int_{-1}^1 d\varepsilon [\psi_{np}^-(\varepsilon)]^* a_{\varepsilon\sigma} . \end{aligned} \quad (24)$$

The operators $a_{np\sigma}^{(\dagger)}$ and $b_{np\sigma}^{(\dagger)}$ defined in this way fulfill the usual fermionic commutation relations. The Hamiltonian Eq. (18) is now expressed in terms of these discrete operators.

In particular, the transformed hybridization term (first part only) is

$$\int_{-1}^1 d\varepsilon h(\varepsilon) f_{\sigma}^{\dagger} a_{\varepsilon\sigma} = f_{\sigma}^{\dagger} \sum_{np} \left[a_{np\sigma} \int^{+,n} d\varepsilon h(\varepsilon) \psi_{np}^{+}(\varepsilon) + b_{np\sigma} \int^{-,n} d\varepsilon h(\varepsilon) \psi_{np}^{-}(\varepsilon) \right], \quad (25)$$

where we have defined

$$\int^{+,n} d\varepsilon \equiv \int_{x_{n+1}}^{x_n} d\varepsilon, \quad \int^{-,n} d\varepsilon \equiv \int_{-x_n}^{-x_{n+1}} d\varepsilon. \quad (26)$$

For a constant $h(\varepsilon) = h$, the integrals in Eq. (25) filter out the $p = 0$ component only

$$\int^{\pm,n} d\varepsilon h \psi_{np}^{\pm}(\varepsilon) = \sqrt{d_n} h \delta_{p,0}. \quad (27)$$

In other words, the impurity couples only to the $p = 0$ components of the conduction band states. It will become clear soon, that this point was essential in Wilson's original line of arguments, so we would like to maintain this feature ($h(\varepsilon)$ being constant in each interval of the logarithmic discretization) also for a general, non-constant $\Delta(\omega)$. Note that this restriction for the function $h(\varepsilon)$ does not lead to additional approximations for a non-constant $\Delta(\omega)$ as one can shift all the remaining ε -dependence to the dispersion $g(\varepsilon)$, see Eq. (19).

As discussed in [7] in the context of the soft-gap model, one can even set $h(\varepsilon) = h$ for all ε . Here we follow the proposal of [8], that is, we introduce a step function for $h(\varepsilon)$

$$h(\varepsilon) = h_n^{\pm}, \quad x_{n+1} < \pm\varepsilon < x_n, \quad (28)$$

with h_n^{\pm} given by the average of the hybridization function $\Delta(\omega)$ within the respective intervals,

$$h_n^{\pm 2} = \frac{1}{d_n} \int^{\pm,n} d\varepsilon \frac{1}{\pi} \Delta(\varepsilon). \quad (29)$$

This leads to the following form of the hybridization term

$$\int_{-1}^1 d\varepsilon h(\varepsilon) f_{\sigma}^{\dagger} a_{\varepsilon\sigma} = \frac{1}{\sqrt{\pi}} f_{\sigma}^{\dagger} \sum_n [\gamma_n^{+} a_{n0\sigma} + \gamma_n^{-} b_{n0\sigma}], \quad (30)$$

with $\gamma_n^{\pm 2} = \int^{\pm,n} d\varepsilon \Delta(\varepsilon)$.

Next, we turn to the conduction electron term, which transforms into

$$\begin{aligned} \int_{-1}^1 d\varepsilon g(\varepsilon) a_{\varepsilon\sigma}^{\dagger} a_{\varepsilon\sigma} &= \sum_{np} \left(\xi_n^{+} a_{np\sigma}^{\dagger} a_{np\sigma} + \xi_n^{-} b_{np\sigma}^{\dagger} b_{np\sigma} \right) \\ &+ \sum_{n, p \neq p'} \left(\alpha_n^{+}(p, p') a_{np\sigma}^{\dagger} a_{np'\sigma} - \alpha_n^{-}(p, p') b_{np\sigma}^{\dagger} b_{np'\sigma} \right). \end{aligned} \quad (31)$$

The first term on the right hand side of Eq. (31) is diagonal in the index p . The discrete set of energies ξ_n^\pm can be expressed as (see Ref. [8])

$$\xi_n^\pm = \frac{\int^{\pm,n} d\varepsilon \Delta(\varepsilon) \varepsilon}{\int^{\pm,n} d\varepsilon \Delta(\varepsilon)} \left[= \pm \frac{1}{2} \Lambda^{-n} (1 + \Lambda^{-1}) \right], \quad (32)$$

where we give the result for a constant $\Delta(\varepsilon)$ in brackets. The coupling of the conduction band states with different p, p' (the second term) recovers the continuum (no approximation has been made so far, Eq. (31) is still exact). For the case of a linear dispersion, $g(\varepsilon) = \varepsilon$, the prefactors $\alpha_n^\pm(p, p')$ are the same for both sides of the discretization and take the following form

$$\alpha_n^\pm(p, p') = \frac{1 - \Lambda^{-1}}{2\pi i} \frac{\Lambda^{-n}}{p' - p} \exp \left[\frac{2\pi i (p' - p)}{1 - \Lambda^{-1}} \right]. \quad (33)$$

The actual discretization of the Hamiltonian is now achieved by dropping the terms with $p \neq 0$ in the expression for the conduction band Eq. (31). This is, of course, an approximation, the quality of which is not clear from the outset. To motivate this step we can argue that (i) the $p \neq 0$ states couple only indirectly to the impurity (via their coupling to the $p = 0$ states in Eq. (31)) and (ii) the coupling between the $p = 0$ and $p \neq 0$ states has a prefactor $(1 - \Lambda^{-1})$ which vanishes in the limit $\Lambda \rightarrow 1$. In this sense one can view the couplings to the states with $p \neq 0$ as small parameters and consider the restriction to $p = 0$ as zeroth order step in a perturbation expansion with respect to the coefficients $a_n^\pm(p, p')$ [1]. As it turns out, the accuracy of the results obtained from the $p = 0$ states only is surprisingly good even for values of Λ as large as $\Lambda = 2$, so that in all NRG calculations the $p \neq 0$ states have never been considered so far.

Finally, after dropping the $p \neq 0$ terms and relabeling the operators $a_{n0\sigma} \equiv a_{n\sigma}$, etc., we arrive at the discretized Hamiltonian as depicted by Fig. 1b:

$$\begin{aligned} H = & H_{\text{imp}} + \sum_{n\sigma} [\xi_n^+ a_{n\sigma}^\dagger a_{n\sigma} + \xi_n^- b_{n\sigma}^\dagger b_{n\sigma}] \\ & + \frac{1}{\sqrt{\pi}} \sum_{\sigma} f_{\sigma}^\dagger \left[\sum_n (\gamma_n^+ a_{n\sigma} + \gamma_n^- b_{n\sigma}) \right] + \frac{1}{\sqrt{\pi}} \sum_{\sigma} \left[\sum_n (\gamma_n^+ a_{n\sigma}^\dagger + \gamma_n^- b_{n\sigma}^\dagger) \right] f_{\sigma}. \end{aligned} \quad (34)$$

While the various steps leading to the discretized Hamiltonian, Eq. (34), are fairly straightforward from a mathematical point of view, the question may arise here, why are we performing such a specific discretization at all?

Quite generally, a numerical diagonalization of Hamiltonian matrices allows to take into account the various impurity-related terms in the Hamiltonian, such as a local Coulomb repulsion, non-perturbatively. Apparently, the actual implementation of such a numerical diagonalization scheme requires some sort of discretization of the original model, which has a continuum of bath states. There are, however, many ways to discretize such a system, so let me try to explain why the logarithmic discretization is the most suitable one here. As it turns out, quantum impurity models are very often characterized by energy scales orders of magnitudes smaller than the bare energy scales of the model Hamiltonian. If the ratio of these energy scales is, for example, of the order of 10^5 , a linear discretization would require energy intervals of size at most 10^{-6} to

properly resolve the lowest scale in the system. Since for a finite system the splitting of energies is roughly inversely proportional to the system size, one would need of the order of 10^6 sites, which renders an exact diagonalization impossible.

Apparently, the logarithmic discretization reduces this problem in that the low-energy resolution now depends exponentially on the number of sites in the discretized model, so that energy scales of the order of 10^5 (in units of the bandwidth) can be reached by performing calculations for fairly small clusters, say with ≈ 20 sites.

3.2 Mapping on a semi-infinite chain

According to Fig. 1b and c, the next step is to transform the discretized Hamiltonian Eq. (34) into a semi-infinite chain form with the first site of the chain (filled circle in Fig. 1c) representing the impurity degrees of freedom. You will notice, of course, that we have introduced a representation of the siAm in the form of a semi-infinite chain already in Fig. 4, with the Hamiltonian given by Eq. (15). The structure of the Hamiltonian Eq. (15) and the one corresponding to Fig. 1c (see Eq. (38) below) is exactly the same, so why should we distinguish these Hamiltonians at all? The essential point here is that the semi-infinite chain introduced in Sec. 2 is an exact representation of the *original* model, that means it has the same hybridization function as the model in the original site representation, for example, the model for a single impurity coupled to a two-dimensional system as shown in Fig. 3.

In contrast, the semi-infinite chain to be introduced in this subsection corresponds to the discretized Hamiltonian Eq. (34), which is an approximation of the original, continuous model, so the model corresponding to Fig. 1c – for which the expression ‘Wilson chain’ is often used – is an approximation as well. As will be discussed in the following, the main feature of the Wilson chain is that the t_l are falling off exponentially with distance from the impurity.

In the Hamiltonian for the Wilson chain, the impurity directly couples only to one conduction electron degree of freedom with operators $c_{0\sigma}^{(\dagger)}$, the form of which can be directly read off from the second and third line in Eq. (34). With the definition

$$c_{0\sigma} = \frac{1}{\sqrt{\xi_0}} \sum_n [\gamma_n^+ a_{n\sigma} + \gamma_n^- b_{n\sigma}], \quad (35)$$

in which the normalization constant is given by

$$\xi_0 = \sum_n ((\gamma_n^+)^2 + (\gamma_n^-)^2) = \int_{-1}^1 d\varepsilon \Delta(\varepsilon), \quad (36)$$

the hybridization term can be written as

$$\frac{1}{\sqrt{\pi}} f_\sigma^\dagger \sum_n (\gamma_n^+ a_{n\sigma} + \gamma_n^- b_{n\sigma}) = \sqrt{\frac{\xi_0}{\pi}} f_\sigma^\dagger c_{0\sigma}, \quad (37)$$

(similarly for the Hermitian conjugate term). Note that for a coupling to a single site as in Eq. (4), the coupling in Eq. (37) reduces to $\sqrt{\xi_0/\pi} = V$.

The operators $c_{0\sigma}^{(\dagger)}$ are of course not orthogonal to the operators $a_{n\sigma}^{(\dagger)}, b_{n\sigma}^{(\dagger)}$. Constructing a new set of mutually orthogonal operators $c_{n\sigma}^{(\dagger)}$ from $c_{0\sigma}^{(\dagger)}$ and $a_{n\sigma}^{(\dagger)}, b_{n\sigma}^{(\dagger)}$ by a standard Gram-Schmidt procedure leads to the desired chain Hamiltonian, which takes the form

$$H = H_{\text{imp}} + \sqrt{\frac{\xi_0}{\pi}} \sum_{\sigma} \left[f_{\sigma}^{\dagger} c_{0\sigma} + c_{0\sigma}^{\dagger} f_{\sigma} \right] + \sum_{\sigma, n=0}^{\infty} \left[\varepsilon_n c_{n\sigma}^{\dagger} c_{n\sigma} + t_n \left(c_{n\sigma}^{\dagger} c_{n+1\sigma} + c_{n+1\sigma}^{\dagger} c_{n\sigma} \right) \right], \quad (38)$$

with the operators $c_{n\sigma}^{(\dagger)}$ corresponding to the n -th site of the conduction electron part of the chain. The parameters of the chain are the on-site energies ε_n and the hopping matrix elements t_n . The operators $c_{n\sigma}^{(\dagger)}$ in Eq. (38) and the operators $\{a_{n\sigma}^{(\dagger)}, b_{n\sigma}^{(\dagger)}\}$ in Eq. (34) are related via an orthogonal transformation

$$\begin{aligned} a_{n\sigma} &= \sum_{m=0}^{\infty} u_{mn} c_{m\sigma}, & b_{n\sigma} &= \sum_{m=0}^{\infty} v_{mn} c_{m\sigma}, \\ c_{n\sigma} &= \sum_{m=0}^{\infty} [u_{nm} a_{m\sigma} + v_{nm} b_{m\sigma}]. \end{aligned} \quad (39)$$

From the definition of $c_{0\sigma}$ in Eq. (35) we can read off the coefficients u_{0m} and v_{0m}

$$u_{0m} = \frac{\gamma_m^+}{\sqrt{\xi_0}}, \quad v_{0m} = \frac{\gamma_m^-}{\sqrt{\xi_0}}. \quad (40)$$

For the remaining coefficients u_{nm}, v_{nm} , as well as for the parameters ε_n, t_n , one can derive recursion relations following the scheme described in detail in, for example, Appendix A of [9]. The starting point here is the equivalence of the free conduction electron parts

$$\sum_{n\sigma} [\xi_n^+ a_{n\sigma}^{\dagger} a_{n\sigma} + \xi_n^- b_{n\sigma}^{\dagger} b_{n\sigma}] = \sum_{\sigma, n=0}^{\infty} \left[\varepsilon_n c_{n\sigma}^{\dagger} c_{n\sigma} + t_n \left(c_{n\sigma}^{\dagger} c_{n+1\sigma} + c_{n+1\sigma}^{\dagger} c_{n\sigma} \right) \right]. \quad (41)$$

The recursion relations are initialized by the equations

$$\begin{aligned} \varepsilon_0 &= \frac{1}{\xi_0} \int_{-1}^1 d\varepsilon \Delta(\varepsilon) \varepsilon, \\ t_0^2 &= \frac{1}{\xi_0} \sum_m [(\xi_m^+ - \varepsilon_0)^2 (\gamma_m^+)^2 + (\xi_m^- - \varepsilon_0)^2 (\gamma_m^-)^2], \\ u_{1m} &= \frac{1}{t_0} (\xi_m^+ - \varepsilon_0) u_{0m}, \\ v_{1m} &= \frac{1}{t_0} (\xi_m^- - \varepsilon_0) v_{0m}. \end{aligned} \quad (42)$$

For $n \geq 1$, the recursion relations read

$$\begin{aligned} \varepsilon_n &= \sum_m (\xi_m^+ u_{nm}^2 + \xi_m^- v_{nm}^2), \\ t_n^2 &= \sum_m [(\xi_m^+)^2 u_{nm}^2 + (\xi_m^-)^2 v_{nm}^2] - t_{n-1}^2 - \varepsilon_n^2, \\ u_{n+1,m} &= \frac{1}{t_n} [(\xi_m^+ - \varepsilon_n) u_{nm} - t_{n-1} u_{n-1,m}], \\ v_{n+1,m} &= \frac{1}{t_n} [(\xi_m^- - \varepsilon_n) v_{nm} - t_{n-1} v_{n-1,m}]. \end{aligned} \quad (43)$$

Note that for a particle-hole symmetric hybridization function, $\Delta(\omega) = \Delta(-\omega)$, the on-site energies ε_n are zero for all n .

For a general hybridization function, the recursion relations have to be solved numerically. Although these relations are fairly easy to implement, it turns out that the iterative solution breaks down typically after about 20-30 steps. The source of this instability is the wide range of values for the parameters entering the recursion relations (for instance for the discretized energies ξ_m^\pm). In most cases this problem can be overcome by using arbitrary precision routines for the numerical calculations. Furthermore, it is helpful to enforce the normalization of the vectors u_{nm} and v_{nm} after each step.

Analytical solutions for the recursion relations have so far been given only for few special cases. Wilson derived a formula for the t_n for a constant density of states of the conduction electrons in the Kondo version of the impurity model [1]; this corresponds to a constant hybridization function $\Delta(\omega)$ in the interval $[-1, 1]$. Here we have $\varepsilon_n = 0$ for all n and the expression for the t_n reads

$$t_n = \frac{(1 + \Lambda^{-1})(1 - \Lambda^{-n-1})}{2\sqrt{1 - \Lambda^{-2n-1}}\sqrt{1 - \Lambda^{-2n-3}}} \Lambda^{-n/2}. \quad (44)$$

Similar expressions have been given for the soft-gap model, see [8]. In the limit of large n this reduces to

$$t_n \longrightarrow \frac{1}{2} (1 + \Lambda^{-1}) \Lambda^{-n/2}. \quad (45)$$

The fact that the t_n fall off exponentially with the distance from the impurity is essential for the following discussion, so let me briefly explain where this n -dependence comes from. Consider the discretized model Eq. (34) with a finite number $1 + M/2$ (M even) of conduction electron states for both positive and negative energies (the sum over n then goes from 0 to $M/2$). This corresponds to $2 + M$ degrees of freedom which result in $2 + M$ sites of the conduction electron part of the chain after the mapping to the Wilson chain. The lowest energies in the discretized model Eq. (34) are the energies $\xi_{M/2}^\pm$ which, for a constant hybridization function, are given by $\xi_{M/2}^\pm = \pm \frac{1}{2} \Lambda^{-M/2} (1 + \Lambda^{-1})$, see Eq. (32). This energy shows up in the chain Hamiltonian as the last hopping matrix element t_M , so we have $t_M \sim \xi_{M/2}$ equivalent to Eq. (45).

Equation (38) is a specific one-dimensional representation of the siAm with the special feature that the hopping matrix elements t_n fall off exponentially. As mentioned above, this representation is not exact since in the course of its derivation, the $p \neq 0$ terms have been dropped. Nevertheless, the conduction electron sites of the chain do have a physical meaning in the original model as they can be viewed as a sequence of shells centered around the impurity. The first site of the conduction electron chain corresponds to the shell with the maximum of its wavefunction closest to the impurity [1,3]; this shell is coupled to a shell further away from the impurity and so on.

3.3 Iterative diagonalization

The transformations described so far are necessary to map the problem onto a form (the Wilson chain, Eq. (38)) for which an iterative renormalization group (RG) procedure can be defined.

This is the point at which, finally, the RG character of the approach enters.

The chain Hamiltonian Eq. (38) can be viewed as a series of Hamiltonians H_N ($N = 0, 1, 2, \dots$) which approaches H in the limit $N \rightarrow \infty$.

$$H = \lim_{N \rightarrow \infty} \Lambda^{-(N-1)/2} H_N, \quad (46)$$

with

$$H_N = \Lambda^{(N-1)/2} \left[H_{\text{imp}} + \sqrt{\frac{\xi_0}{\pi}} \sum_{\sigma} \left(f_{\sigma}^{\dagger} c_{0\sigma} + c_{0\sigma}^{\dagger} f_{\sigma} \right) + \sum_{\sigma, n=0}^N \varepsilon_n c_{n\sigma}^{\dagger} c_{n\sigma} + \sum_{\sigma, n=0}^{N-1} t_n \left(c_{n\sigma}^{\dagger} c_{n+1\sigma} + c_{n+1\sigma}^{\dagger} c_{n\sigma} \right) \right]. \quad (47)$$

The factor $\Lambda^{(N-1)/2}$ in Eq. (47) (and, consequently, the factor $\Lambda^{-(N-1)/2}$ in Eq. (46)) has been chosen to cancel the N -dependence of t_{N-1} , the hopping matrix element between the last two sites of H_N . Such a scaling is useful for the discussion of fixed points, as described below. For a different n -dependence of t_n , as for the spin-boson model [9], the scaling factor has to be changed accordingly. (The n -dependence of ε_n is, in most cases, irrelevant for the overall scaling of the many-particle spectra.)

Two successive Hamiltonians are related by

$$H_{N+1} = \sqrt{\Lambda} H_N + \Lambda^{N/2} \left[\sum_{\sigma} \varepsilon_{N+1} c_{N+1\sigma}^{\dagger} c_{N+1\sigma} + \sum_{\sigma} t_N \left(c_{N\sigma}^{\dagger} c_{N+1\sigma} + c_{N+1\sigma}^{\dagger} c_{N\sigma} \right) \right], \quad (48)$$

and the starting point of the sequence of Hamiltonians is given by

$$H_0 = \Lambda^{-1/2} \left[H_{\text{imp}} + \sum_{\sigma} \varepsilon_0 c_{0\sigma}^{\dagger} c_{0\sigma} + \sqrt{\frac{\xi_0}{\pi}} \sum_{\sigma} \left(f_{\sigma}^{\dagger} c_{0\sigma} + c_{0\sigma}^{\dagger} f_{\sigma} \right) \right].$$

This Hamiltonian corresponds to a two-site cluster formed by the impurity and the first conduction electron site. Note that in the special case of the siAm, one can also choose $H_{-1} = \Lambda^{-1} H_{\text{imp}}$ as the starting point (with a proper renaming of parameters and operators) since the hybridization term has the same structure as the hopping term between the conduction electron sites.

The recursion relation Eq. (48) can now be understood in terms of a renormalization group transformation R :

$$H_{N+1} = R(H_N). \quad (49)$$

In a standard RG transformation, the Hamiltonians are specified by a set of parameters \vec{K} and the mapping R transforms the Hamiltonian $H(\vec{K})$ into another Hamiltonian of the same form, $H(\vec{K}')$, with a new set of parameters \vec{K}' . Such a representation does not exist, in general, for the H_N which are obtained in the course of the iterative diagonalization to be described below. Instead, we characterize H_N , and thereby also the RG flow, directly by the many-particle energies $E_N(r)$

$$H_N |r\rangle_N = E_N(r) |r\rangle_N, \quad r = 1, \dots, N_s, \quad (50)$$

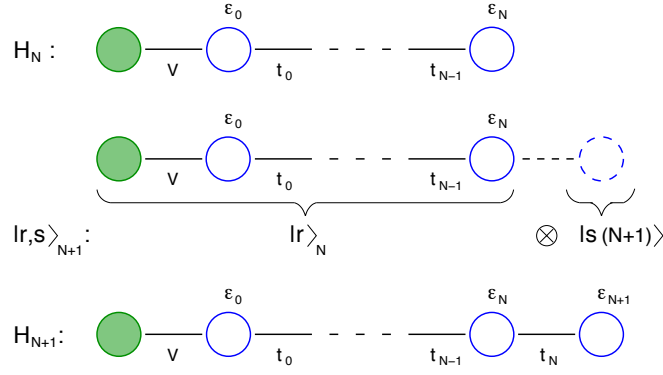


Fig. 6: In each step of the iterative diagonalization scheme one site of the chain (with operators $c_{N+1}^{(\dagger)}$ and on-site energy ε_{N+1}) is added to the Hamiltonian H_N . A basis $|r; s\rangle_{N+1}$ for the resulting Hamiltonian, H_{N+1} , is formed by the eigenstates of H_N , $|r\rangle_N$, and a basis of the added site, $|s(N+1)\rangle$. Figure taken from Ref. [4].

with the eigenstates $|r\rangle_N$ and N_s the dimension of H_N . This is particularly useful in the crossover regime between different fixed points, where a description in terms of an effective Hamiltonian with certain renormalized parameters is not possible. Only in the vicinity of the fixed points (except for certain quantum critical points) one can go back to an effective Hamiltonian description, as described below.

Our primary aim now is to set up an iterative scheme for the diagonalization of H_N , in order to discuss the flow of the many-particle energies $E_N(r)$. Let us assume that, for a given N , the Hamiltonian H_N has already been diagonalized, as in Eq. (50). We now construct a basis for H_{N+1} , as sketched in Fig. 6:

$$|r; s\rangle_{N+1} = |r\rangle_N \otimes |s(N+1)\rangle. \quad (51)$$

The states $|r; s\rangle_{N+1}$ are product states consisting of the eigenbasis of H_N and a suitable basis $|s(N+1)\rangle$ for the added site (the new degree of freedom). From the basis Eq. (51) we construct the Hamiltonian matrix for H_{N+1} :

$$H_{N+1}(rs, r's') = {}_{N+1}\langle r; s | H_{N+1} | r'; s' \rangle_{N+1}. \quad (52)$$

For the calculation of these matrix elements it is useful to decompose H_{N+1} into three parts

$$H_{N+1} = \sqrt{\Lambda} H_N + \hat{X}_{N,N+1} + \hat{Y}_{N+1}, \quad (53)$$

(see, for example, Eq. (48)) where the operator \hat{Y}_{N+1} only contains the degrees of freedom of the added site, while $\hat{X}_{N,N+1}$ mixes these with the ones contained in H_N . Apparently, the structure of the operators \hat{X} and \hat{Y} , as well as the equations for the calculation of their matrix elements, depend on the model under consideration.

The following steps are illustrated in Fig. 7: In Fig. 7a we show the many-particle spectrum of H_N , that is the sequence of many-particle energies $E_N(r)$. Note that, for convenience, the ground-state energy has been set to zero. Figure 7b shows the overall scaling of the energies by the factor $\sqrt{\Lambda}$, see the first term in Eq. (48).

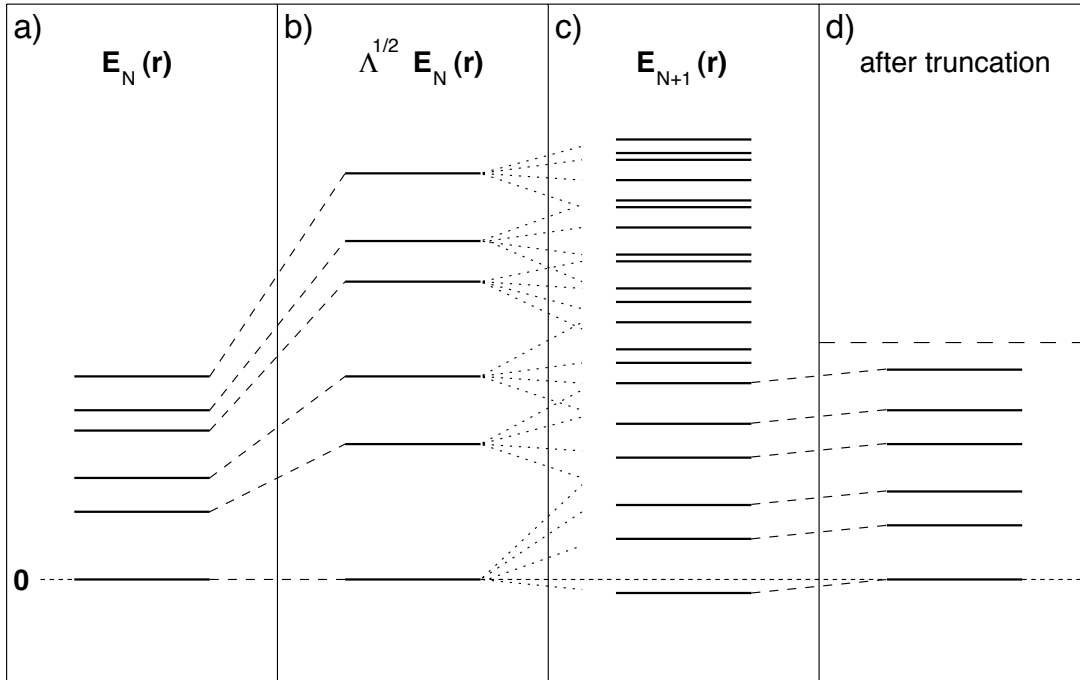


Fig. 7: (a): Many-particle spectrum $E_N(r)$ of the Hamiltonian H_N with the ground-state energy set to zero. (b): The relation between successive Hamiltonians, Eq. (48), includes a scaling factor $\sqrt{\Lambda}$. (c) Many-particle spectrum $E_{N+1}(r)$ of H_{N+1} , calculated by diagonalizing the Hamiltonian matrix Eq. (52). (d) The same spectrum after truncation where only the N_s lowest-lying states are retained; the ground-state energy has again been set to zero. Figure taken from Ref. [4].

Diagonalization of the matrix Eq. (52) gives the new eigenenergies $E_{N+1}(w)$ and eigenstates $|w\rangle_{N+1}$ which are related to the basis $|r; s\rangle_{N+1}$ via the unitary matrix U :

$$|w\rangle_{N+1} = \sum_{rs} U(w, rs) |r; s\rangle_{N+1}. \quad (54)$$

The set of eigenenergies $E_{N+1}(w)$ of H_{N+1} is displayed in Fig. 7c (the label w can now be replaced by r). Apparently, the number of states increases by adding the new degree of freedom (when no symmetries are taken into account, the factor is just the dimension of the basis $|s(N+1)\rangle$). The ground-state energy is negative, but will be set to zero in the following step.

The increasing number of states is, of course, a problem for the numerical diagonalization; the dimension of H_{N+1} grows exponentially with N , even when we consider symmetries of the model so that the full matrix takes a block-diagonal form with smaller submatrices. This problem can be solved by a very simple truncation scheme: after diagonalization of the various submatrices of H_{N+1} one only keeps the N_s eigenstates with the lowest many-particle energies. In this way, the dimension of the Hilbert space is fixed to N_s and the computation time increases linearly with the length of the chain. Suitable values for the parameter N_s depend on the model; for the siAm, N_s of the order of a few hundred is sufficient to get converged results for the many-particle spectra, but the accurate calculation of static and dynamic quantities usually requires larger values of N_s . The truncation of the high energy states is illustrated in Fig. 7d.

Such an ad-hoc truncation scheme needs further explanations. First of all, there is no guarantee that this scheme will work in practical applications and its quality should be checked for each individual application. Important here is the observation that the neglect of the high-energy states does not spoil the low-energy spectrum in subsequent iterations – this can be easily seen numerically by varying N_s . The influence of the high-energy on the low-energy states is small since the addition of a new site to the chain can be viewed as a perturbation of relative strength $\Lambda^{-1/2} < 1$. This perturbation is small for large values of Λ but for $\Lambda \rightarrow 1$ it is obvious that one has to keep more and more states to get reliable results. This also means that the accuracy of the NRG results is getting worse when N_s is kept fixed and Λ is reduced (vice versa, it is sometimes possible to improve the accuracy by *increasing* Λ for fixed N_s).

From this discussion we see that the success of the truncation scheme is intimately connected to the special structure of the chain Hamiltonian (that is $t_n \propto \Lambda^{-n/2}$) which in turn is due to the logarithmic discretization of the original model. A direct transformation of the siAm to a semi-infinite chain as in Eq. (15) results in $t_n \rightarrow \text{const}$ [3], and the above truncation scheme fails.

Let us now be a bit more specific on how to construct the basis $|r; s\rangle_{N+1}$. For this we have to decide, first of all, which of the symmetries of the Hamiltonian should be used in the iterative diagonalization. In the original calculations of Ref. [1] and Refs. [10, 11] the following quantum numbers were used: total charge Q (particle number with respect to half-filling), total spin S and z -component of the total spin S_z . It was certainly essential in the 1970's to reduce the size of the matrices and hence the computation time as much as possible by invoking as many symmetries as possible. This is no longer necessary to such an extent on modern computer systems, i.e. one can, at least for single-band models, drop the total spin S and classify the subspaces with the quantum numbers (Q, S_z) only. This simplifies the program considerably as one no longer has to worry about reduced matrix elements and the corresponding Clebsch-Gordan coefficients, see, for example [10]. The $|r; s\rangle_{N+1}$ are then constructed as:

$$\begin{aligned}
 |Q, S_z, r; 1\rangle_{N+1} &= |Q + 1, S_z, r\rangle_N, \\
 |Q, S_z, r; 2\rangle_{N+1} &= c_{N+1\uparrow}^\dagger |Q, S_z - \frac{1}{2}, r\rangle_N, \\
 |Q, S_z, r; 3\rangle_{N+1} &= c_{N+1\downarrow}^\dagger |Q, S_z + \frac{1}{2}, r\rangle_N, \\
 |Q, S_z, r; 4\rangle_{N+1} &= c_{N+1\uparrow}^\dagger c_{N+1\downarrow}^\dagger |Q - 1, S_z, r\rangle_N.
 \end{aligned} \tag{55}$$

Note that the quantum numbers (Q, S_z) on each side of these equations refer to different systems: on the left-hand side they are for the system including the added site, and on the right-hand side without the added site. We do not go into the details of how to set up the Hamiltonian matrices Eq. (52), as this procedure is described in great detail in Appendix B of Ref. [10].

For fermionic baths, the discretization parameter Λ and the number of states N_s kept in each iteration are the only parameters which govern the quality of the results of the NRG procedure. For a bosonic bath, the infinite dimensional basis $|s(N+1)\rangle$ for the added bosonic site requires an additional parameter N_b , which determines the dimension of $|s(N+1)\rangle$.

3.4 Renormalization group flow

The result of the iterative diagonalization scheme are the many-particle energies $E_N(r)$ with $r = 1, \dots, N_s$ (apparently, the number of states is less than N_s for the very first steps before the truncation sets in). The index N goes from 0 to a maximum number of iterations, N_{\max} , which usually has to be chosen such that the system has approached its low-temperature fixed point.

As illustrated in Fig. 7, the set of many-particle energies cover roughly the same energy range independent of N , due to the scaling factor $\Lambda^{(N-1)/2}$ in Eq. (47). The energy of the first excited state of H_N is of the order of $\Lambda^{(N-1)/2}t_{N-1}$, a constant according to Eq. (45). The energy of the highest excited state kept after truncation depends on N_s – for typical parameters this energy is approximately 5-10 times larger than the lowest energy.

Multiplied with the scaling factor $\Lambda^{-(N-1)/2}$, see Eq. (46), the energies $E_N(r)$ are an approximation to the many-particle spectrum of the Wilson chain Eq. (38) within an energy window decreasing exponentially with increasing N . Note, that the energies for higher lying excitations obtained for early iterations are not altered in later iteration steps due to the truncation procedure. Nevertheless one can view the resulting set of many-particle energies and states from all NRG iterations N as approximation to the spectrum of the full Hamiltonian and use them to calculate physical properties in the whole energy range.

Here we want to focus directly on the many-particle energies $E_N(r)$ and show how one can extract information about the physics of a given model by analyzing their flow, that is the dependence of $E_N(r)$ on N .

As a typical example for such an analysis, we show in Fig. 8 the flow of the many-particle energies for the symmetric siAm, with parameters $\varepsilon_f = -0.5 \cdot 10^{-3}$, $U = 10^{-3}$, $V = 0.004$, and $\Lambda = 2.5$ (the same parameters as used in Fig. 5 of Ref. [10]; note that we show here a slightly different selection of the lowest-lying states). The energies are plotted for odd N only, that is an odd total number of sites (which is $N+2$). This is necessary, because the many-particle spectra show the usual even-odd oscillations of a fermionic finite-size system (the patterns for even N look different but contain, of course, the same physics). The data points are connected by lines to visualize the flow. As in Ref. [10], the many-particle energies are labeled by total charge Q and total spin S .

What is the information one can extract from such a flow diagram? First of all we note the appearance of three different fixed points of the RG transformation for early iteration numbers $N < 10$, for intermediate values of N and for $N > 60$ (strictly speaking, because we look at N odd only, these are fixed points of R^2 , not of R). The physics of these fixed points cannot be extracted by just looking at the pattern of the many-particle energies. This needs some further analysis, in particular the direct diagonalization of fixed point Hamiltonians (which usually have a simple structure) and the comparison of their spectrum with the numerical data. An excellent account of this procedure for the symmetric and asymmetric siAm has been given in Refs. [10, 11], and there is no need to repeat this discussion here. The analysis shows that for $N \approx 3 - 9$, the system is very close to the free-orbital fixed point, with the fixed point Hamiltonian given by Eq. (38) for $\varepsilon_f = 0$, $U = 0$, and $V = 0$. This fixed point is unstable and

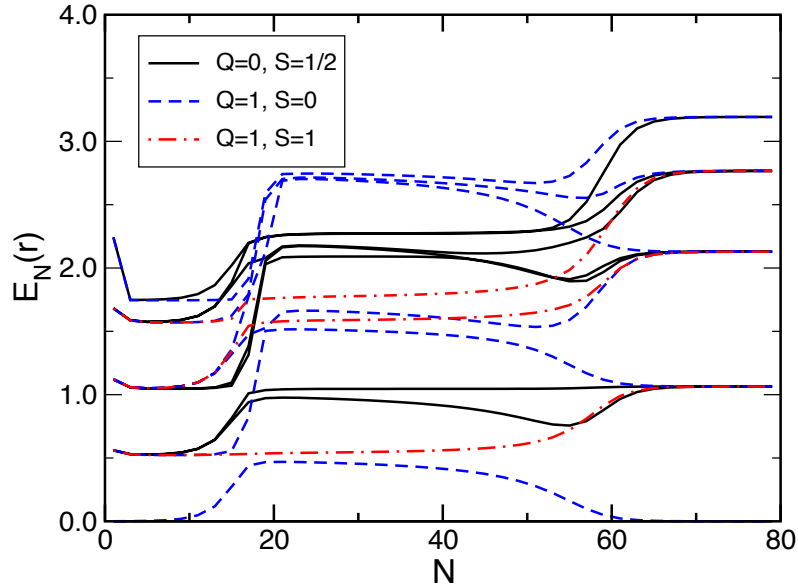


Fig. 8: Flow of the lowest-lying many-particle energies of the single-impurity Anderson model for parameters $\varepsilon_f = -0.5 \cdot 10^{-3}$, $U = 10^{-3}$, $V = 0.004$, and $\Lambda = 2.5$. The states are labeled by the quantum numbers total charge Q and total spin S . See the text for a discussion of the fixed points visible in this plot. Figure taken from Ref. [4].

for $N \approx 11 - 17$, we observe a rapid crossover to the local-moment fixed point. This fixed point is characterized by a free spin decoupled from the conduction band (here we have $\varepsilon_f = -U/2$, $U \rightarrow \infty$, and $V = 0$). The local-moment fixed point is unstable as well and after a characteristic crossover (see the discussion below) the system approaches the stable strong-coupling fixed point of a screened spin (with $\varepsilon_f = -U/2$ and $V^2/U \rightarrow \infty$). Note that the terminology ‘strong-coupling’ has been introduced originally because the fixed point Hamiltonian can be obtained from the limit $V \rightarrow \infty$, so ‘coupling’ here refers to the hybridization, not the Coulomb parameter U .

The NRG does not only allow to match the structure of the numerically calculated fixed points with those of certain fixed point Hamiltonians. One can in addition identify the deviations from the fixed points (and thereby part of the crossover) with appropriate perturbations of the fixed point Hamiltonians. Again, we refer the reader to Refs. [10, 11] for a detailed description of this analysis. The first step is to identify the leading perturbations around the fixed points. The leading operators can be determined by expressing them in terms of the operators which diagonalize the fixed point Hamiltonian; this tells us directly how these operators transform under the RG mapping R^2 . One then proceeds with the usual classification into relevant, marginal, and irrelevant perturbations. The final results of this analysis perfectly agree with the flow diagram of Fig. 8: There is a relevant perturbation which drives the system away from the free-orbital fixed point, but for the local-moment fixed point there is only a marginally relevant perturbation, therefore the system only moves very slowly away from this fixed point. Note that this marginal perturbation – which is the exchange interaction between the local moment and the spin of the first conduction electron site – gives rise to the logarithms observed in various physical quan-

ties. Finally, there are only irrelevant operators which govern the flow to the strong-coupling fixed point. These are responsible for the Fermi-liquid properties at very low temperatures [3]. Flow diagrams as in Fig. 8 also give information about the relevant energy scales for the crossover between the fixed points. For example, an estimate of the Kondo temperature T_K (the temperature scale which characterizes the flow to the strong-coupling fixed point) is given by $T_K \approx \omega_c \Lambda^{-\bar{N}/2}$, with $\bar{N} \approx 55$ for the parameters in Fig. 8.

4 Final remarks

The main purpose of these lecture notes was to give a brief introduction to the basic steps of the NRG method, that is the logarithmic discretization (Sec. 3.1), the mapping onto a semi-infinite chain (Sec. 3.2), and the iterative diagonalization (Sec. 3.3). A number of improvements of these technical steps have been introduced since the development of the method by Wilson [1] and I just want to mention a few here.

The discreteness of the model Eq. (34) can be (in some cases) problematic for the calculation of physical quantities. As it is not possible in the actual calculations to recover the continuum by taking the limit $\Lambda \rightarrow 1$ (or by including the $p \neq 0$ terms), it has been suggested to average over various discretizations for fixed Λ [12–14]. The discretization points are then modified as

$$x_n = \begin{cases} 1 & : n = 0 \\ \Lambda^{-(n+Z)} & : n \geq 1, \end{cases} \quad (56)$$

where Z covers the interval $[0, 1)$. This ‘ Z -averaging’ indeed removes certain artificial oscillations.

Another shortcoming of the discretized model is that the hybridization function $\Delta(\omega)$ is systematically underestimated. It is therefore convenient to multiply $\Delta(\omega)$ with the correction factor

$$A_\Lambda = \frac{1}{2} \ln \Lambda \frac{\Lambda + 1}{\Lambda - 1}, \quad (57)$$

which accelerates the convergence to the continuum limit. For a recent derivation of this correction factor, see [15].

The equations for the recursive calculation of the parameters of the semi-infinite chain, the $\{\varepsilon_n\}$ and $\{t_n\}$ in Eq. (38), have been given in Sec. 3.2, but it is certainly not obvious how to arrive at analytical expressions as in Eq. (44) (for the special case of constant $\Delta(\omega)$). This issue has been discussed in more general terms in Ref. [16]. By using the theory of orthogonal polynomials, expressions for the parameters $\{\varepsilon_n\}$ and $\{t_n\}$ can now be given for more complex hybridization functions, like the ones appearing in the Ohmic and sub-Ohmic spin-boson model.

Another technical improvement to be mentioned here is about the truncation of basis states in the iterative diagonalization of the Wilson chain. It is not at all clear how many states one should keep here and the convergence is usually checked by repeating the calculation for various values of N_s . A quantitative criterion to analyze the convergence, based on the discarded weight in the reduced density matrices, has been recently given in Ref. [17].

The physics of the siAm, in particular the Kondo effect, has been mentioned here only in the context of the renormalization group flow of the many-particle levels (Sec. 3.4). To actually see the screening of the local moment by the conduction electrons, one has to calculate an appropriate physical quantity, for example the magnetic susceptibility. Some extra care has to be taken to calculate such quantities, for more details, see Sec. III in Ref. [4]. As an example of the technical difficulties one has to solve to obtain reliable data for the specific heat, see the recent paper Ref. [18].

The starting point for the NRG is the integral representation Eq. (18), which is just one possible representation of the siAm. In Sec. 2 you have seen that there are many different ways to represent the model which are all equivalent provided they give the same hybridization function $\Delta(\omega)$. We have discussed that the siAm can always be viewed as a single-channel model. As a side remark, note that for multi-impurity Anderson models it is not at all trivial to count the number of screening channels. So far this has been done only for a few special cases.

There is a wide range of models and physical phenomena to which the NRG has been applied (for an overview, see Secs. 4 and 5 in Ref. [4]). To conclude, here is a list of a few very recent applications:

- Real-space charge densities and their connection to the Kondo-screening cloud [19].
- Real-time dynamics in quantum impurity systems [20].
- Steady-state currents through nanodevices [21].
- Transport through multi-level quantum dots [22].
- Multi-channel and multi-impurity physics [23].
- Zero-bias conductance in carbon nanotube quantum dots [24].

Acknowledgments

I would like to thank Theo Costi and Thomas Pruschke, the coauthors of the NRG-review [4] on which part of these lecture notes are based, for many helpful discussions, and Andrew Mitchell for carefully reading the manuscript. Funding from the Deutsche Forschungsgemeinschaft through SFB 608 and FOR 960 is gratefully acknowledged.

References

- [1] K.G. Wilson, *Rev. Mod. Phys.* **47**, 773 (1975)
- [2] E. Pavarini, E. Koch, D. Vollhardt, and A. Lichtenstein (eds.):
The LDA+DMFT approach to strongly correlated materials,
Reihe Modeling and Simulation, Vol. 1 (Forschungszentrums Jülich, 2011)
<http://www.cond-mat.de/events/correl11>
- [3] Alex C. Hewson: *The Kondo Problem to Heavy Fermions*,
(Cambridge University Press, Cambridge, England, 1993)
- [4] R. Bulla, T.A. Costi, and Th. Pruschke, *Rev. Mod. Phys.* **80**, 395 (2008)
- [5] P.W. Anderson, *Phys. Rev.* **124**, 41 (1961)
- [6] R. Bulla, A.C. Hewson, and Th. Pruschke, *J. Phys.: Condens. Matter* **10**, 8365 (1998)
- [7] K. Chen and C. Jayaprakash, *J. Phys.: Condens. Matter* **7**, L491 (1995)
- [8] R. Bulla, Th. Pruschke, and A.C. Hewson, *J. Phys.: Condens. Matter* **9**, 10463 (1997)
- [9] R. Bulla, H.-J. Lee, N.-H. Tong, and M. Vojta, *Phys. Rev. B* **71**, 045122 (2005)
- [10] H.R. Krishna-murthy, J.W. Wilkins, and K.G. Wilson, *Phys. Rev. B* **21**, 1003 (1980)
- [11] H.R. Krishna-murthy, J.W. Wilkins, and K.G. Wilson, *Phys. Rev. B* **21**, 1044 (1980)
- [12] H.O. Frota and L.N. Oliveira, *Phys. Rev. B* **33**, 7871 (1986)
- [13] M. Yoshida, M.A. Whitaker, and L.N. Oliveira, *Phys. Rev. B* **41**, 9403 (1990)
- [14] W.C. Oliveira and L.N. Oliveira, *Phys. Rev. B* **49**, 11986 (1994)
- [15] V.L. Campo Jr. and L.N. Oliveira, *Phys. Rev. B* **72**, 104432 (2005)
- [16] A.W. Chin, Á. Rivas, S.F. Huelga, and M.B. Plenio, *J. Math. Phys.* **51**, 092109 (2010)
- [17] A. Weichselbaum, *Phys. Rev. B* **84**, 125130 (2011)
- [18] L. Merker and T.A. Costi, preprint arXiv:1206.3201 (2012)
- [19] A.K. Mitchell, M. Becker, and R. Bulla, *Phys. Rev. B* **84**, 115120 (2011)
- [20] F.B. Anders and A. Schiller, *Phys. Rev. Lett.* **95**, 196801 (2005)
- [21] F.B. Anders, *Phys. Rev. Lett.* **101**, 066804 (2008)
- [22] D.E. Logan, C.J. Wright, and M.R. Galpin, *Phys. Rev. B* **80**, 125117 (2009)

- [23] E. Sela, A.K. Mitchell, and L. Fritz, Phys. Rev. Lett. **106**, 147202 (2011);
A.K. Mitchell, E. Sela, and D.E. Logan, Phys. Rev. Lett. **108**, 086405 (2012)
- [24] F.B. Anders, D.E. Logan, M.R. Galpin, and G. Finkelstein,
Phys. Rev. Lett. **100**, 086809 (2008)